The Astrophysical Journal, 740:83 (10pp), 2011 October 20 doi:10.1088/0004-637X/740/2/83

STARS AND IONIZED GAS IN THE S0 GALAXY NGC 7743: AN INCLINED LARGE-SCALE GASEOUS DISK*

Ivan Yu. Katkov[1], Alexei V. Moiseev[2], and Olga K. Sil'chenko[1,3]
[1] Sternberg Astronomical Institute, Moscow 119992, Russia; katkov.ivan@gmail.com
[2] Special Astrophysical Observatory, Russian Academy of Sciences, Nizhnii Arkhyz, Karachaevo-Cherkesskaya Republic 369167, Russia; moisav@gmail.com
[3] Isaac Newton Institute of Chile, Moscow Branch, Russia; olga@sai.msu.su
Received 2011 January 7; accepted 2011 June 24; published 2011 October 3

ABSTRACT

We used deep, long-slit spectra and integral-field spectral data to study the stars, ionized gas kinematics, and stellar population properties in the lenticular barred galaxy NGC 7743. We show that ionized gas at distances larger than 1.5 kpc from the nucleus settles in the disk, which is significantly inclined toward the stellar disk of the galaxy. Making different assumptions about the geometry of the disks and including different sets of emission lines in the fitting, under the assumption of thin, flat-disk circular rotation, we obtain the full possible range of angles between the disks to be $34^\circ \pm 9^\circ$ or $77^\circ \pm 9^\circ$. The most probable origin of the inclined disk is the external gas accretion from a satellite orbiting the host galaxy, with a corresponding angular momentum direction. The published data on the H I distribution around NGC 7743 suggest that the galaxy has a gas-rich environment. The emission-line ratio diagrams imply the domination of shock waves in the ionization state of the gaseous disk, whereas the contribution of photoionization from recent star formation seems to be negligible. In some parts of the disk, a difference between the velocities of the gas emitting from the forbidden lines and Balmer lines is detected. This may be caused by the mainly shock-excited inclined disk, whereas some fraction of the Balmer-line emission is produced by a small amount of gas excited by young stars in the main stellar disk of NGC 7743. In the circumnuclear region ($R < 200$ pc), some evidence of the active galactic nucleus jet's interaction with an ambient interstellar medium was found.

Key words: galaxies: elliptical and lenticular, cD – galaxies: individual (NGC 7743) – galaxies: interactions – galaxies: ISM – galaxies: kinematics and dynamics

Online-only material: color figures

1. INTRODUCTION

Interactions play an important role in galaxy evolution. Even a minor merger with a mass ratio less than 1/5–1/10, which does not disturb the overall structure of the galaxy disk, may cause a gas concentration in its central region, triggering nuclear activity or a nuclear starburst. According to the hierarchical paradigm, such events happen many times during a galaxy's lifetime; however, it is difficult to detect minor merging footprints, even recent ones, against the background of a high-surface-brightness galaxy. Deep images, revealing low-contrast tidal features (see, e.g., Martínez-Delgado et al. 2010; Smirnova et al. 2010), or detailed studies of the stellar populations and internal kinematics of the galaxy are required.

The consequences of a minor merger may be quite diverse. The gas of a larger galaxy may be disturbed by a satellite intrusion, and the gas may flow into the center, resulting in strong gas compression in the nucleus and a subsequent nuclear star formation burst. A rather young current age of the nuclear star population inside an older bulge may be the signature of such an event. If the initial direction of the orbital angular momentum of the satellite significantly differs from the main galaxy disk-rotation momentum, then some fraction of stars or gas clouds in the galaxy may be rotating on orbits tilted (or orthogonal to) toward the main galactic disk, or even counter-rotating within it. Long-slit and integral-field spectral observations gave much evidence of kinematical misalignments in circumnuclear regions of early-type disk galaxies, including kinematically decoupled cores. Numerous examples and detailed discussion and references can be found, for instance, in the papers by Afanasiev et al. (1989), Corsini et al. (2003), Moiseev et al. (2004), Sarzi et al. (2006), and Coccato et al. (2007). Unfortunately, observational evidence of large-scale (beyond the 1 kpc central region), kinematically decoupled subsystems is still quite rare (see Sil'chenko et al. 2009 and references therein). Therefore, every new example of similarly peculiar objects is interesting.

In this paper, we demonstrate that the main fraction of the ionized gas in NGC 7743 rotates on the orbits, considerably inclined toward the main stellar disk of the galaxy, which may be a result of external gas accretion or tidal destruction of a small gas-rich companion. The paper is organized as follows: Section 2 gives an overview of the literature on previous studies of the galaxy, Section 3 describes the spectroscopic observations and data reduction process, Section 4 considers the properties of the stellar population (kinematics, age, and metallicity), Section 5 contains a study of gas kinematics and ionization states, and Section 6 includes an overall discussion of the structure and kinematics of NGC 7743.

2. NGC 7743: WHAT WAS KNOWN BEFORE?

NGC 7743 is a barred early-type galaxy (NED morphological type (R)SB0$^+$(s)) with a total blue luminosity of $M_B = -19.4$ (according to the HyperLeda database[4]). Following Jensen et al. (2003), we adopt the distance to the galaxy to be 19.2 Mpc, which corresponds to a linear scale of 93 pc arcsec^{-1}.

* Based on the observations collected with the 6-m telescope of the Special Astrophysical Observatory of the Russian Academy of Sciences, which is operated under the financial support of the Science Department of Russia (registration number 01-43).

[4] http://leda.univ-lyon1.fr

Table 1
Log of the Observations

Instrument	Date	P.A. (deg)	Sp. Range (Å)	Sp. Resolution (Å)	Exp. Time (s)	Seeing (″)
SCORPIO	2007 Sep 21	268	4800–5550	2.5	9 × 1200	1.9
	2009 Jan 22	268	6100–7100	3.1	2 × 500	2.4
	2007 Sep 21	358	4800–5550	2.5	9 × 1200	1.8
	2009 Jan 22	358	6100–7100	3.1	2 × 400	3.0
	2008 Dec 19	313	4800–5550	2.5	8 × 1200	1.2
	2009 Oct 15	220	6100–7100	3.1	10 × 1200	1.6
SAURON	2007 Aug 14	355 (Pos. 1)	4800–5400	4.8	2 × 1800	2
	2007 Aug 14	355 (Pos. 2)	4800–5400	4.8	2 × 1800	2

A smooth, two-armed spiral structure without any traces of star formation dominates in optical images of the galaxy. According to Ho et al. (1997), the galaxy has an active nucleus of the Sy2 type. Radio observations reveal a compact (under the beam = 1″–5″), non-thermal source in the nucleus (Nagar et al. 1999; Ho & Ulvestad 2001). However, nuclear activity is not very high. Alonso-Herrero et al. (2000), using their spectral observations, classified NGC 7743 as a "low-luminosity AGN (active galactic nucleus)" and noted that the optical emission-line ratios correspond to the boundary case between the Sy2 and LINER activity types. The X-ray observations by Terashima et al. (2002) also suggest relatively low activity in the NGC 7743 nucleus compared with other Seyfert galaxies from their sample.

Hubble Space Telescope (*HST*) imaging reveals the complex structure of the circumnuclear region (R < 300–500 pc), where emission knots and several curved dust lanes are observed (Regan & Mulchaey 1999). Martini et al. (2003) described this structure as a loosely-wound circumnuclear spiral. Moiseev et al. (2004) used integral-field spectroscopy to study inner-region morphology and kinematics. They suggested that a turn of the innermost isophotes relates to the circumnuclear dust spiral rather than to a triaxial bulge, as was claimed earlier. Despite the relatively low intensity of emission lines, they succeeded in obtaining some conclusions about the ionized gas kinematics. In the region of R < 2″–4″ (190–370 pc), the gas motions agreed in general with the stellar disk rotation, but non-circular ionized gas motions were also detected locally, south of the nucleus. Moiseev et al. (2004) also suggested that the inner part of the galaxy disk can be tilted with respect to the outer disk.

Radio observations by Duprie & Schneider (1996) demonstrated a very low amount of neutral gas (near their detection limit) in the NGC 7743 disk through the ∼3′ beam, whereas two separate H I clouds were discovered in the immediate neighborhood of the galaxy, with masses of $M_{\rm H\,I} = 6.4 \times 10^7\,M_\odot$ and $4.5 \times 10^8\,M_\odot$. Their systemic velocities were 1610 km s^{-1} and 1509 km s^{-1}, respectively, which are close to the NGC 7743 systemic velocity of 1710 km s^{-1} (HyperLeda). According to the NED database, these clouds are associated with the galaxies KUG 2341+097 and LSBC F750-04, with projected distances of 8.′3 (46 kpc) and 11.′0 (61 kpc) from NGC 7743. The absolute magnitude of the brighter galaxy (KUG 2341+097) is about $M_B = -16$. Therefore, NGC 7743 is surrounded by satellites that, together, contain neutral hydrogen one order larger than the disk of the main galaxy. At the same time, Maiolino et al. (1997), from their radio observations with a beam = 55″, detected CO emission corresponding to the total mass of the molecular gas in the galaxy disk of about $1.3 \times 10^8\,M_\odot$, which is comparable with the H I mass in the local environment of NGC 7743.

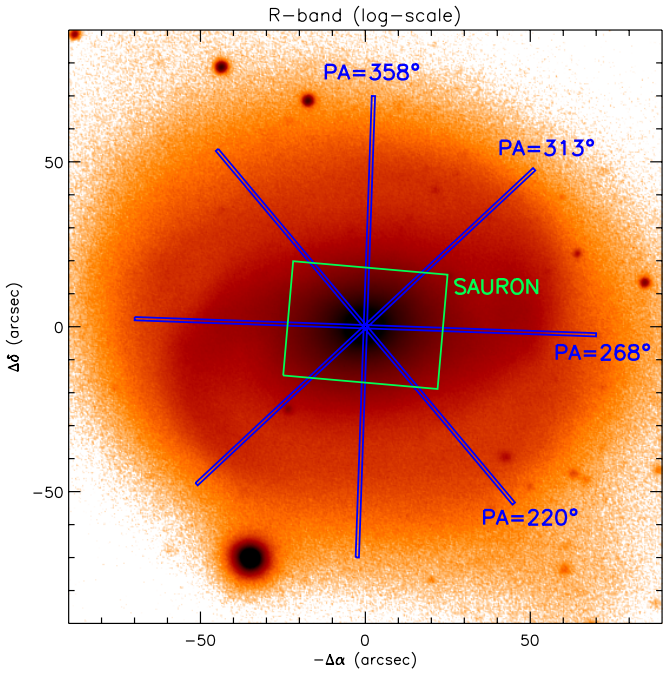

Figure 1. Positions of the SCORPIO slits and the SAURON mosaic field of view are overlapped onto the *R*-band image of the galaxy NGC 7743 from Moiseev et al. (2004).

(A color version of this figure is available in the online journal.)

3. SPECTRAL OBSERVATIONS AND DATA REDUCTION

In our study of NGC 7743, we used two types of spectral data. Long-slit spectroscopy with long-enough exposures allows observations of the very outer parts of the galaxy disk; however, the one-dimensional character of the long-slit data restricts consideration of any azimuthal variations. Integral-field spectroscopy (so-called three-dimensional spectroscopy) provides two-dimensional mapping of kinematical and stellar population characteristics, but only for the central part of the galaxy due to a limited field of view.

3.1. SCORPIO Long-slit Observations

Spectral observations were made at the prime focus of the Special Astrophysical Observatory of the Russian Academy of Sciences 6-m telescope with the multimode focal reducer SCORPIO (Afanasiev & Moiseev 2005). The slit was 6.′1 in length and 1″ in width. The 2048 × 2048 EEV 42-40 CCD provided a scale of 0.35 arcsec pixel^{-1} along the slit. The log of observations is given in Table 1 and the slit positions on the galaxy image are shown in Figure 1.

The first observations, in 2007, were performed to study the stellar kinematics (the PI of the proposal was Anatoly Zasov); therefore, the "green" spectral range of 4800–5550 Å was chosen. It contains strong stellar absorption-line features as well as ionized gas emission lines—Hβ and [O III]$\lambda\lambda$4959, 5007. After preliminary analysis of these data, a difference in the kinematics of gas and stars was found, and we carried out additional observations in the "red" spectral domain of 6100–7100 Å, including the brighter emission lines—Hα, [N II]$\lambda\lambda$6548, 6583, and [S II]$\lambda\lambda$6716, 6731.

The spectra were reduced in the standard way using our IDL-based software (see, for instance, Zasov et al. 2008). For the night sky spectrum subtraction, we applied an advanced technique that took into account the variations of the line-spread function (LSF) along the slit (Katkov & Chilingarian 2011). The model of the LSF was derived from the twilight sky spectra which were observed the same nights as the galaxy was, before and after the galaxy observations. These spectra were binned by 10 pixels along the slit, and the wavelength range was divided into six segments. The LSF parameters were estimated over every segment by fitting the observed spectrum to a broadened high-resolution spectrum of the Sun using the ULySS software[5] (Koleva et al. 2008b, 2009) adapted for the SCORPIO data.

Further data analysis included the following steps.

1. Adaptive binning along the slit—we summed spectra to achieve the minimal value of signal-to-noise ratio (S/N) = 20–30.
2. Masking the emission-line regions and fitting the binned galaxy spectra to the simple stellar population (SSP) model PEGASE.HR (Le Borgne et al. 2004), convolved with a parametric line-of-sight velocity distribution (LOSVD), using ULySS software. The resulting stellar physical parameters are the line-of-sight velocity v, velocity dispersion σ, higher-order Gauss–Hermite moments h_3, h_4, and the SSP-equivalent luminosity-weighted parameters: the age T and metallicity [Z/H]. The stellar population models were constructed from the local star spectra library, and therefore the element abundance ratios, [Mg/Fe] in particular, cannot be free variables. Although we deal with a rather high model metallicity, [Fe/H] > -0.4, the model alpha-element-to-iron ratio is necessarily close to the solar ratio due to the fixed chemical properties of the stars in the Sun's neighborhood. For a more detailed description, see Koleva et al. (2008b, 2009).
3. Subtracting the stellar contribution from non-binned spectra using the model's stellar spectra, evaluated in every bin at the previous step and normalized here by a polynomial approximation of the surface brightness distribution. The result is a non-binned ionized gas spectrum.
4. Adaptive binning of the emission-line spectra. The bins were formed under the condition that S/N > 10 for the targeted emission line.
5. Fitting the emission lines using Gaussians convolved with the LSF. For the doublets of [O III], [N II], and [S II], the rest-frame separation between components, their widths, and their intensity ratios (except the sulfur lines) were fixed.

It should be noted that the cross-sections P.A. $= 268^\circ$ and 358° in the "red" spectral range were observed with relatively low exposure times, and emission-line measurements in these spectra gave no additional information about the ionized gas kinematics with respect to the deep spectra in the "green" spectral domain. Therefore, we used the measurements of the emission lines Hα, [N II], and [S II] in these P.A.s only to derive the ionization-state diagrams. In contrast, in P.A. $= 220^\circ$ (the galaxy's minor axis), we used very deep "red" spectra, where the ionized gas emission lines were detected at large distances from the nucleus. At the same time, the estimations of the stellar population parameters in the "red" domain are uncertain, in contrast to the "green" spectra.

The kinematical profiles of the stellar and gaseous components, the emission-line ratios, and the radial profiles of the stellar population parameters are shown in Figure 2.

3.2. SAURON Integral-field Spectroscopy

We also included data from the 4.2-m William Herschel Telescope integral-field spectrograph SAURON (Bacon et al. 2001), obtained in the framework of the ATLAS3D survey (Cappellari et al. 2011). We retrieved the raw data from the open Isaac Newton Group Archive, which is maintained as part of the CASU Astronomical Data Centre at the Institute of Astronomy, Cambridge. NGC 7743 was observed in two positions of the SAURON lenslet array, $33'' \times 41''$ in size and centered on opposite sides relative to the galactic nucleus. The resulting central part of the galaxy observed was $35'' \times 50''$ (see Figure 1), with $0\farcs94$ sampling. For our analysis, we used the scientific-ready spectral data cubes that were presented earlier by Sil'chenko & Chilingarian (2011).

The data cubes were fitted with the ULySS software package in the same manner as the long-slit data described above. The model of the LSF constructed from the twilight-sky spectra was taken into account. Because of the relatively low S/N of the emission lines, we simultaneously fitted Hβ and [O III] emission-line profiles by assuming that their velocities were the same; the line widths and intensities were free parameters. The maps were smoothed by a Gaussian with FWHM = 1.5 pixels. The resulting maps are presented in Figure 3.

4. STELLAR CONTENT

4.1. Kinematics

Radial variations in the v and σ derived from our long-slit data (Figure 2) show good agreement with the SAURON maps over the central galaxy region (Figure 3). The line-of-sight velocity curve at P.A. $= 313^\circ$ (which corresponds to the kinematical major axis; see below) has a sharp small-amplitude internal maximum at $R \approx 2''$ (190 pc). At larger radii, the rotation velocity rises continuously up to $R \approx 60''$ (5.5 kpc). The apparent amplitude of the stellar rotation velocity is about 160 km s^{-1}.

We assumed a purely Gaussian shape of the LOSVD and ignored the contribution of the h_3 and h_4 moments because the value of the intrinsic velocity dispersion is comparable to the width of the LSF ($\sigma_{\rm LSF} \approx 65$ km s^{-1}). The σ profiles along different P.A.s are slightly different: the cross-sections along P.A. $= 313^\circ$ and 358° reveal a peak of 80 km s^{-1} achieved in the nucleus, while along the bar (P.A. $= 268^\circ$) a central plateau appears. A complex surface distribution of the σ is confirmed by the SAURON maps (Figure 3): in the central region ($R < 5''$), σ is depressed with respect to the neighboring regions. Similar "σ drop" features in barred galaxies may result from circumnuclear, dynamically cold young stellar disks (Wozniak et al. 2003). Koleva et al. (2008a) also noted that such a σ depression can be an artifact related to the template

[5] http://ulyss.univ-lyon1.fr/

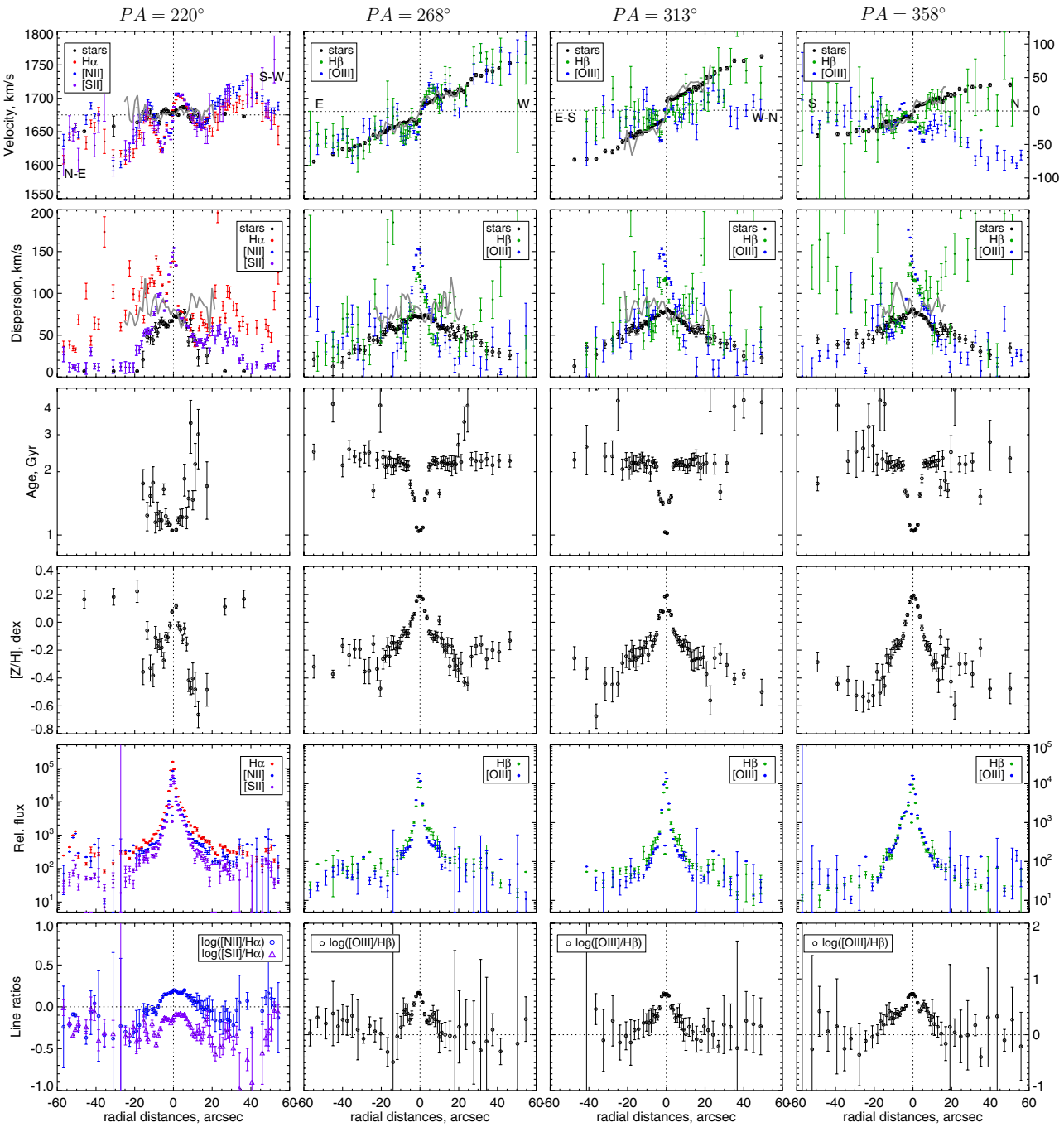

Figure 2. Results of the long-slit observations. Each column corresponds to the slit position angle labeled at the top. Data for P.A. = 220° are shown for the "red" spectral range, and in other cases we present the results only for the "green" spectral domain. From top to bottom, we show the radial distributions of the line-of-sight velocity, the velocity dispersion, the age and metallicity of the stellar component, the intensity of the emission lines (in arbitrary units), and the line intensity ratios. Gray lines correspond to the pseudo-slits extracted from the IFU data.

(A color version of this figure is available in the online journal.)

mismatch. However, in the case of NGC 7743, we propose an interpretation of the σ drop in the framework of the Wozniak et al. (2003) concept because the presence of a young stellar population in the galaxy core is confirmed by our measurements (see the next subsection). We also think that in our case we have no problems with template mismatch: the inspection of the residuals after model spectra subtraction gives an impression of the fitting quality (Figure 4). Note that our estimate of the central velocity dispersion is slightly lower than those of other authors: HyperLeda gives 84.5 ± 2.4 km s^{-1} averaged over six measurements.

The kinematical orientation parameters were determined by applying a model of thin, flat circular rotation to the observed velocity fields. The model corresponds to

$$V_{\rm obs} = V_{\rm sys} + V_{\rm rot}(R)\frac{\cos\varphi\sin i}{\sqrt{\sec^2 i - \cos^2\varphi\tan^2 i}}$$

$$R = r\sqrt{\sec^2 i - \cos^2\varphi\tan^2 i},$$

where R and r are, respectively, the radius of the galaxy plane and the radius of the plane of the sky, and i is the inclination of

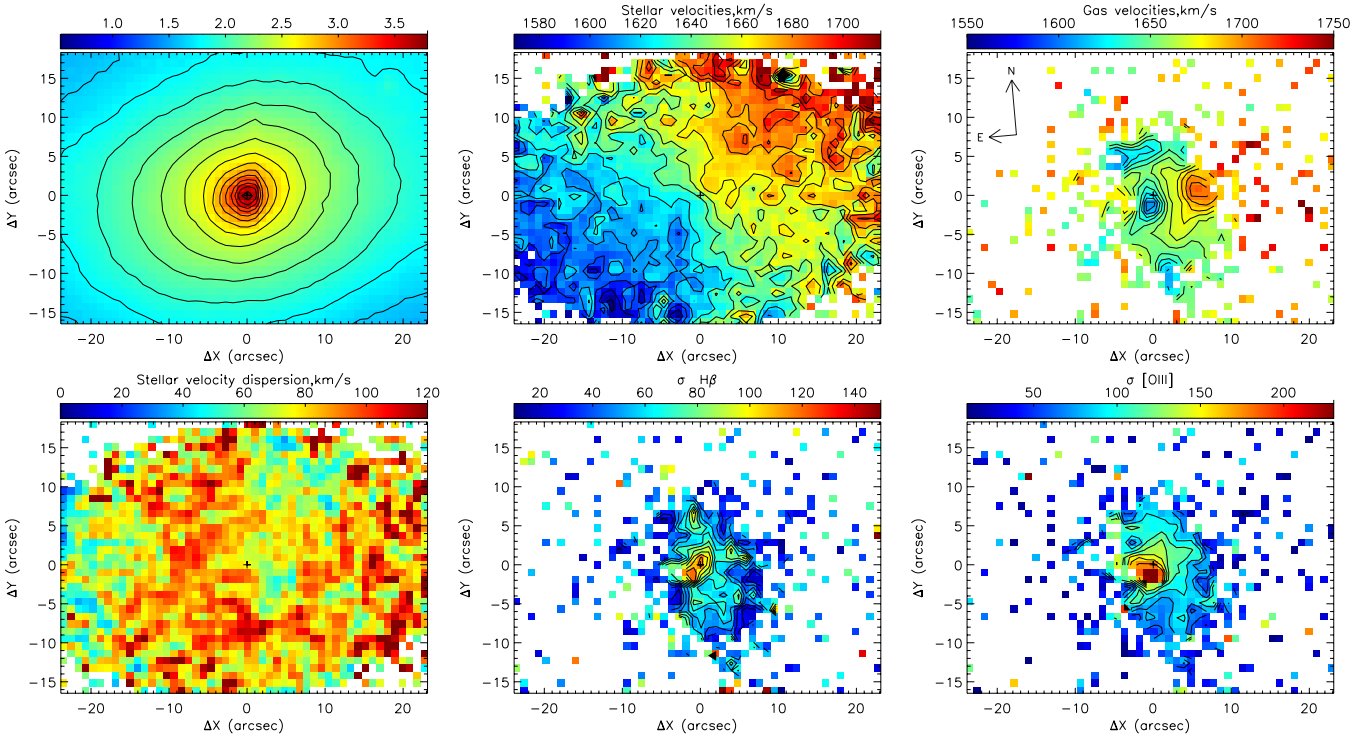

Figure 3. Results of the SAURON data analysis. The top row shows the continuum image and the line-of-sight velocity fields for the stars and ionized gas. The bottom row shows the map of the stellar component velocity dispersion and velocity dispersion maps for the lines Hβ and [O III].

(A color version of this figure is available in the online journal.)

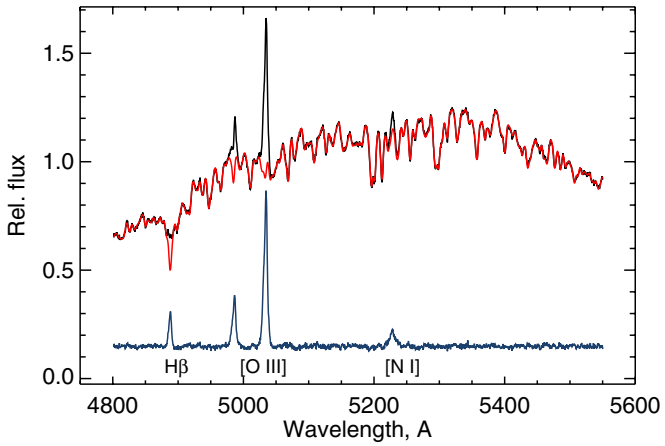

Figure 4. Comparison between the observed spectrum (black line) at $r = -2''$ into cross-section P.A.$_{\rm slit} = 313^\circ$ and the model of the stellar population (red line). The blue line represents a residual between the observed spectrum and model 1.

(A color version of this figure is available in the online journal.)

the galaxy plane. The position angle of the kinematical major axis of the stellar disk (i.e., the disk line of nodes) P.A.$_0$ and angle φ are related by $\varphi = {\rm P.A.}_{\rm slit} - {\rm P.A.}_0$. The rotation curve $V_{\rm rot}(R)$ was determined via several fixed radial nodes, and was then interpolated to all radii using spline functions. Thus, the model parameters are the rotation velocity values at fixed radial nodes, the common inclination, and the line-of-nodes position angle. We simultaneously fitted three long-slit stellar velocity profiles (the most extensive measurements being in the "green" domain) and the SAURON velocity field. The best model has an inclination of $i_{\rm star} = 40^\circ \pm 2^\circ$ and a major axis position angle of P.A.$_{\rm star} = 310^\circ \pm 5^\circ$. The rotation curve is shown in Figure 5 (left column). Moiseev et al. (2004) found P.A.$_{\rm star} = 300^\circ$–310° from the circumnuclear velocity field of stars ($R < 7''$), which almost coincides with our new measurements for the entire large-scale stellar disk. It is important to note that the large-scale bar could perturb the circular velocities of stars; however, we have found that these perturbations are negligible in the case of NGC 7743. It follows from the tilted-ring analysis of the SAURON velocity field (for the method description, see Moiseev et al. 2004) that radial variations in the kinematical major axis P.A. demonstrate very small deviations (1°–2°) from the mean P.A.$_{\rm star}$ (cited above) up to $R = 25''$ (2.3 kpc). Such a picture would have been impossible if the bar had significantly distorted the velocity field—we should observe a turn of the P.A. along the radius because the bar's potential contribution decreases with distance from the center, while in the very center the rotation of the bulge dominates the line-of-sight velocity field. On the other hand, we tried to search for the orientation parameters, excluding the bar area and using only the elements with $R > 30''$ (2.8 kpc). This fit returns a value of P.A.$_{\rm star}$ roughly equal to the estimates given above, but the inclination cannot be confidently determined in this fit.

4.2. Age and Metallicity

Radial variations in the stellar population parameters derived for NGC 7743 from our long-slit data—those of SSP-equivalent age and metallicity—are given in Figure 2, together with the other radial profiles. The stellar nucleus of NGC 7743 appears to be chemically and evolutionarily decoupled: the mean stellar age in the nucleus is only 1 Gyr and the metallicity is 1.5 times above solar. Beyond the nucleus, metallicity drops to subsolar values and the age stabilizes at about 2.5 Gyr. We suppose that our measurements at $R < 20''$–$30''$ (i.e., 1.9–2.8 kpc) relate

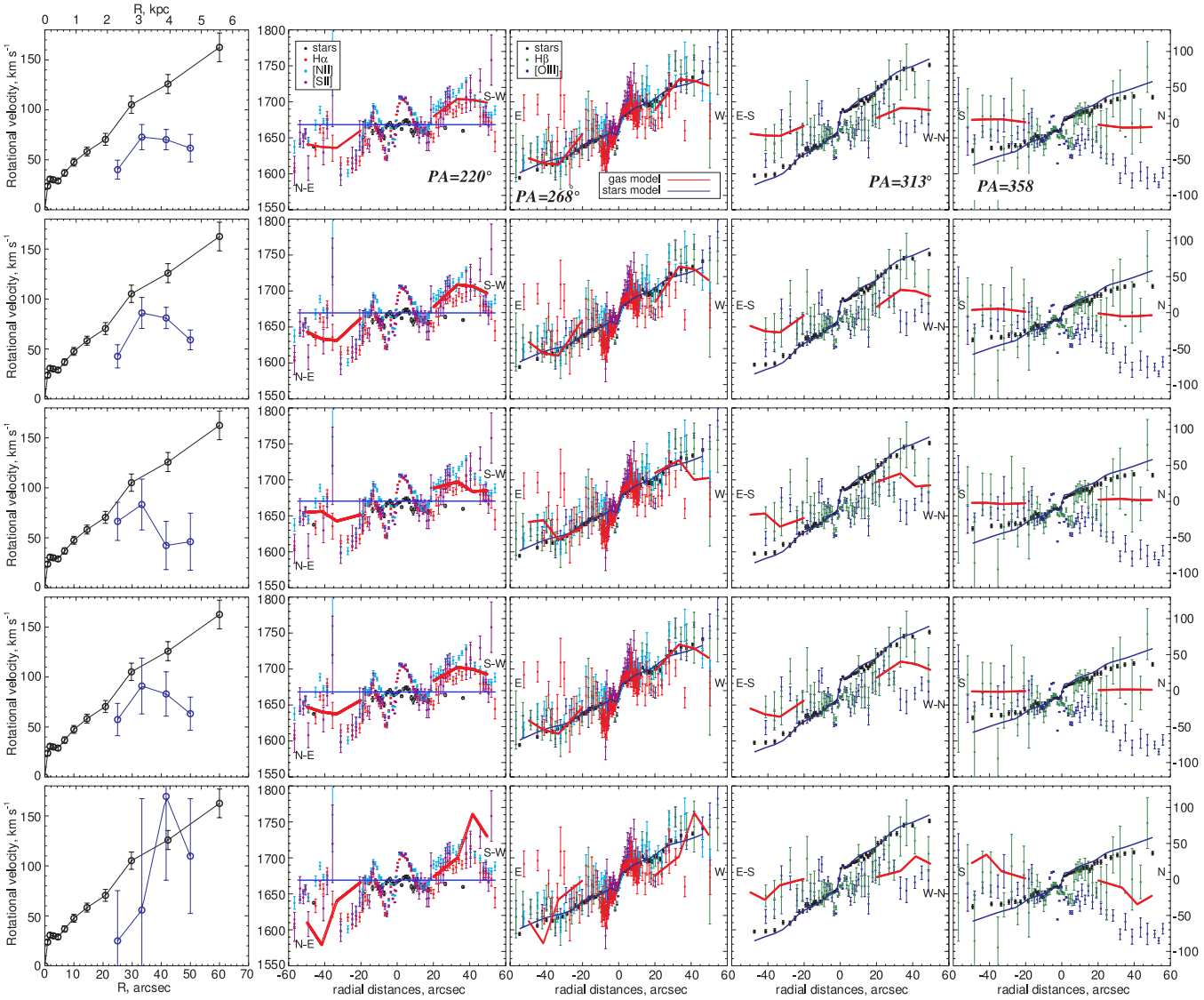

Figure 5. Series of experiments to determine the circularly rotating model of a thin disk to the outer gas. Each row corresponds to the model configuration described in Table 2—Nos. 1 to 5 from top to bottom, respectively. The left column shows the stellar rotational model (black lines and circles) and the gaseous one (blue lines and circles). The following columns correspond to different cross-sections. Black circles represent line-of-sight stellar velocity, while colored circles represent gaseous velocity. The blue and red lines show the stellar and gaseous rotation model projections to different cross-sections, respectively.

(A color version of this figure is available in the online journal.)

mainly to the bulge and bar of NGC 7743, based on its surface brightness distribution (Erwin et al. 2008).

Earlier, we reported the chemical and evolutionary distinctions of the nucleus of NGC 7743 with our integral-field spectroscopic results for the central part of the galaxy. Obtaining data via the Multi-Pupil Fiber Spectrograph (MPFS) of the Russian 6-m telescope, Sil'chenko (2006) measured the Lick indices and found that the nucleus was five times more metal rich and more than 2 Gyr younger than the neighboring bulge. However, the absolute values of the ages and metallicities obtained here differ from those obtained by Sil'chenko (2006): there, [Z/H] = +0.7 was found for the nucleus and 0.0 for the bulge, and the mean age of the bulge was determined to be 4 Gyr. The emission lines were very strong in the nuclear and circumnuclear spectra, and the excitation mechanism of those was unclear, so perhaps the correction of the Lick index Hβ for the emission by Sil'chenko (2006) was not completely correct. Hence, the stellar population parameters for NGC 7743 in Sil'chenko (2006) may be biased. Later, Sil'chenko & Chilingarian (2011) analyzed the SAURON data (which are analyzed here as well) using direct spectrum fitting in the pixel area, which allows one to exclude all spectral regions affected by emission. The results of the SAURON data analysis by Sil'chenko & Chilingarian (2011) agree almost perfectly with the present results derived by fitting the long-slit SCORPIO spectra: they obtained [Z/H] = +0.2 and an age of 1.2 Gyr for the nucleus, and [Z/H] = −0.33 and 2.2 Gyr for the bulge (Sil'chenko & Chilingarian 2011), while Figure 2 implies [Z/H] = +0.2 and T = 1 Gyr in the nucleus and [Z/H] = -0.3 ± 0.1 and 2.5 Gyr for the bulge. Therefore, the data of several spectrographs give evidence for the young age and enhanced metallicity of the stellar nucleus of NGC 7743; we conclude that there is a signature of a recent nuclear star formation burst.

In Figure 2, the stellar population parameter profile of P.A. = 268°, almost along the bar, is quite outstanding compares to the others. The semiaxis of the bar is 31″–37″ (2.9–3.4 kpc)

Table 2
Determination of the Gaseous Disk Orientation

No.	Emission Lines	Cross-sections	i (deg)	P.A. (deg)	δi_1	δi_2
1	All	All	62	257	45 ± 14	89 ± 15
2	Forbidden lines [O III], [N II], [S II]	All	47	261	34 ± 12	78 ± 14
3	Balmer lines Hβ, Hα	All	42	273	24 ± 11	77 ± 15
4	All	P.A.$_{\rm slit}$ = 220, 268	43	270	26 ± 11	77 ± 14
5	All	P.A.$_{\rm slit}$ = 313, 358	38	244	40 ± 11	64 ± 13

according to the estimates by Erwin (2005). At the slit orientation along the bar, unlike the other two profiles, the metallicity does not diminish toward the measurement limits but stops its fall at a radius of about 30″, near the end of the bar, and then rises a little. Perhaps here we feel the influence of the so-called ansae—the bright and often star-forming regions at the ends of a bar that are especially frequent in barred galaxies of early morphological types (Laurikainen et al. 2007)—additional star formation should increase simultaneously the continuum surface brightness and the mean stellar metallicity.

5. IONIZED GAS

5.1. Gas Velocities

Gas motions in NGC 7743 are more complex than those of the stars and appear decoupled in all position angles except P.A. = 268° (Figure 2). Along P.A. = 358°, the velocity projections onto our line of sight have opposite winding senses for the gas and for the stars. By using the SAURON data, we constructed the well-sampled two-dimensional ionized-gas velocity field, but only for the very inner region, $R < 8''$ (740 pc). Meanwhile, due to long exposures and adaptive binning application, from the SCORPIO/long-slit data, we derived emission-line velocities up to the edge of the stellar velocity measurements—toward 60″ (5.6 kpc) from the center.

Close to the minor axis of the stellar disk (P.A. = 220°), where the stellar rotation velocity projections are almost zero, the gas line-of-sight velocity oscillates with an amplitude of 50–70 km s^{-1}. Inspecting the SAURON-based gas velocity field, we see a "blue" velocity spot at 1″–2″ (i.e., 90–190 pc) south of the nucleus; this peculiar region is discussed below, in Section 5.3. Trying to reconcile the gas velocity profiles of four position angles, we conclude that the ionized-gas motions inside the central kiloparsec are quite different from those in the outer disk. Within $R < 10''$ (900 pc), at least two mechanisms affecting the gas motions can be identified: an active-nucleus impact and non-circular velocities induced by the circumnuclear spiral wave, which settles perhaps off the stellar disk plane. At the same time, the outer gas rotates rather regularly, though in a different plane from that of the stars.

We performed a series of calculations in the circularly rotating model of a thin disk for the outer gas (at $R = 25''$–$50''$, 2.3–4.7 kpc), alternately excluding different cross-sections and emission lines and using the same formulae as described in Section 4.1.

The considered configurations (combinations of the emission lines in different cross-sections) are listed in Table 2. Figure 5 shows the comparison of the model rotation curves (blue lines) with the observed line-of-sight velocities for every long-slit cross-section. The first configuration (the top row of Figure 5) includes all available cross-sections. It shows good agreement with the data from P.A. = 220° and P.A. = 268°, but it is mismatched with the observed velocities in the W-N (P.A. = 313°) and N (P.A. = 358°) sides of the galaxy's disk. The main problem arises from significant differences in the velocities estimated in the Hβ and [O III] emission lines (see discussion below). For this reason, we also considered separately fitting for the forbidden ([O III], [S II], [N II]) and Balmer (Hα, Hβ) emission lines; see corresponding configurations 2 and 3. Note that the resulting rotation curve in case 2 seems to be more realistic compared with the abrupt decrease in rotation velocities in case 3. This may be related to the fact that some part of the Balmer emission is produced by the main disk (see below). We also considered the numerical stability of our fitting using different combinations of cross-sections. In configuration 4, we excluded points along P.A. = 313° and 358°, with the most dramatic difference appearing between the ionized gas kinematics in the forbidden and Balmer lines. In contrast, in configuration 5, only points from the P.A. = 313° and 358° cross-sections were used.

Further, we determined the angle between the stellar and gaseous disks using the following formula (Moiseev 2008):

$$\cos \delta i = \cos(\mathrm{P.A.}_{\rm gas} - \mathrm{P.A.}_{\rm star}) \sin i_{\rm star} \sin i_{\rm gas} + \cos i_{\rm star} \cos i_{\rm gas}.$$

Here, we assume that $i < 90°$ if the angular momentum vector is directed toward the observer, while in the opposite momentum direction the inclination is $180° - i$. Supposing that the large-scale spiral arms in the stellar disk are trailing, we determine $i_{\rm star} = 40°$. However, for the gaseous disk, we cannot choose between the alternate directions of its angular momentum vector. Hence, for the mutual inclination angle, we obtain two possible solutions, δi_1 and δi_2. Table 2 presents the resulting parameters of different configurations.

The mutual inclination angles for all configurations considered here are in agreement with each other within the error bar. In any case (see the last two columns of Table 2), the large-scale gaseous disk appears to be strongly inclined toward the main symmetry plane of the galaxy. The mean values for these angles, averaged over all our experiments, are $\delta i_1 = 34° \pm 9°$ and $\delta i_2 = 77° \pm 9°$. Here, the errors correspond to rms. We adopted these values as the possible mutual inclination angles between the stellar and the gaseous disks.

Meanwhile, the difference between the rotation planes of the gas, emitting mostly from the forbidden lines (shock-excited gas) and prominently in the Balmer lines (star-formation-excited gas), may be real. Also, we think that the difference in the orientation parameters of the two groups of cross-sections (experiment numbers 4 and 5 in Table 2) may be physically motivated: perhaps, to the south of the line of nodes at P.A.$_{\rm gas}$ = 220°–270°, we mainly see the inclined, shock-excited gaseous disk, and, to the north of the line of nodes, this inclined gaseous disk is seen through the gas-poor disk of NGC 7743, possibly illuminated by a small number of young stars.

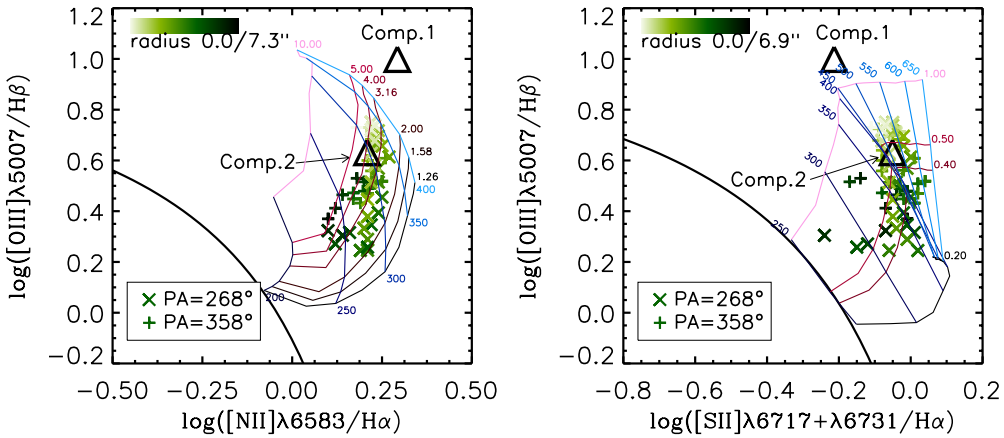

Figure 6. Excitation diagnostic diagrams comparing the emission-line intensity ratios: [O III]/Hβ vs. [N II]/Hα (left) and [O III]/Hβ vs. [S II]/Hα (right). The pluses and crosses mark different long-slit cross-sections. The intensity of the green color corresponds to increasing distance from the center of the sky plane. The solid black curve, which separates the areas with the AGN-induced excitations from areas with star-formation-induced excitations, is taken from Kewley et al. (2001). Our measurements are overlaid by the shock-excitation model (Allen et al. 2008) for the electron density of $n_e = 0.1$ cm^{-3} and solar element abundances. The red color traces magnetic parameter isolines, while the blue color traces the shock velocity isolines. Black triangles mark two separate emission-line components for the regions with clear emission-line splitting; "Comp. 1" relates to the blueshifted component and "Comp. 2" relates to the main one.

(A color version of this figure is available in the online journal.)

5.2. Gas Ionization Sources

To identify the source of gas ionization, we plot our measurements for the inner part of the galaxy, where several emission lines of various excitation degrees are measurable, onto the classical excitation-type diagnostic diagrams (Figure 6). We do not need to take into account the intrinsic reddening because we use the intensity ratios of close pairs of emission lines. One can see (Figure 6) that all measurements are located in the AGN-ionization area of the diagrams. With increasing distance from the center, the contribution of the non-thermal source to gas excitation diminishes because the [O III]λ5007 intensity decreases and the observed points cross the border between the AGN-type and LINER-type excitations ([O III]/Hβ = 3; Veilleux & Osterbrock 1987). The off-center measurements can be fitted best by recent models of shock excitation of low-density gas (*shock + precursor*; Allen et al. 2008) if one supposes a moderate value of the magnetic parameter B and a shock-wave speed of more than 250km s^{-1}.

Therefore, while in the vicinity of the nucleus, gas ionization is mainly produced by an active non-thermal radiation source; 300–500 pc from the center, the main contributors to ionization are the shock waves. Perhaps one of the local producers of the shock waves is the jet of the active nucleus (discussed below). For more distant parts of the gaseous disk, it is reasonable to associate shock waves with the inclined orbits of the gas clouds, which must collide with the interstellar medium of the main large-scale stellar disk (even if the density of the latter is very low). Moreover, a shock wave may be induced by a simple gas cloud, crossing the potential well of the stellar disk—quite analogous to the shock being induced by a gas cloud, crossing a spiral density wave in large-scale disks of spiral galaxies. This mechanism was discussed by Wakamatsu (1993), who considered shock-wave generation in the gas of polar-ring galaxies. To support the latter hypothesis, we can refer to the measurements along P.A. = 220°, where we trace the emission-line intensity ratios toward the largest distance from the center. At the radii of $R = 20''$–$55''$ (1.9–5.1 kpc), we obtain log [N II]/H$\alpha > -0.3$, which excludes photoionization by young stars (Stasińska et al. 2006). Therefore, throughout the entire large-scale gaseous disk of NGC 7743, the gas is ionized by shock waves.

5.3. Jet–Cloud Interaction

Figure 2 shows that the velocity dispersion of ionized gas in the center of NGC 7743 exceeds that of the stellar component by two-fold; evidently, it is an active-nucleus effect. Moreover, in the long-slit cross-sections along P.A. = 313° and P.A. = 358°, the gas velocity dispersion peaks are displaced from the (optical) nucleus by 1″–2″ (i.e., by 90–190 pc), and the gas line-of-sight velocity drops at this radius. The SAURON maps reveal this displacement even better: in Figure 3, one can see a "blue" velocity spot and the gas velocity dispersion peak at 2″ to the south of the nucleus. Within this "spot," the emission-line profiles in the SAURON spectra look asymmetric, and the SCORPIO spectra, which have better spectral resolution, allow one to decompose the entire profiles into two emission-line components (Figure 7). We simultaneously fitted the emission-line profiles for Hβ, [O III], [N II], Hα, and [S II] via a set of Gaussians, broadened with the LSF, by requiring the same velocity difference between two components for all species. The best fit is presented in Figure 7; the more intense component of all lines (Comp. 2) corresponds to regularly rotating gas, and the faint emission-line components (Comp. 1) are blueshifted by 299 ± 8 km s^{-1}. Big black triangles in Figure 6 show intensity ratios for the two components separately. One can see that the ratio of [O III]/Hβ in the off-nuclear Comp. 1 is higher than that in the entire disk, and it is even higher than that in the close vicinity of the active nucleus. A similar picture—a high-speed strong shock excitation along with non-circular motions of gas in a local off-centered area—was observed by Smirnova & Moiseev (2010) in the Seyfert galaxy Mrk 334; this area was identified as a point of a satellite fragment crossing the galaxy's disk. Another consequence of such a crossing is the lower gas density in this "hole" than in the neighboring disk. However, in NGC 7743, the blueshifted Comp. 1 reveals a very high electron density, 3000 ± 1500 cm^{-3}, which is determined from the intensity ratio of [S II]λ6717/[S II]λ6731, while the regularly rotating disk (Comp. 2) only has a density of $n_e = 150 \pm 30$ cm^{-3}. Therefore, in this peculiar region we detect

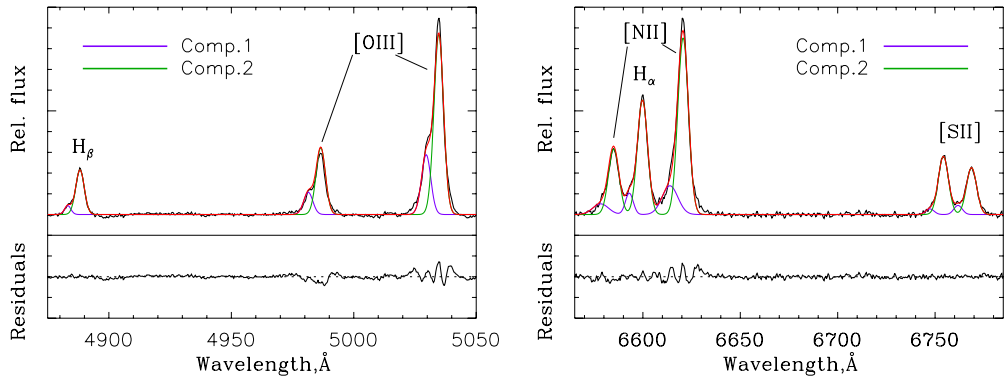

Figure 7. Multi-component emission-line profile, obtained by integrating the long-slit data within the range of $R = -4''$–$0''$ along the cross-section in P.A. = 358°. The black line shows the observed emission-line spectrum after subtracting the model of stellar spectra. The blue line corresponds to the Gaussian-profile model of the blueshifted component ("Comp. 1"), the green line corresponds to the Gaussian-profile model of the main emission component ("Comp. 2"), and the red line traces the full model profile.

(A color version of this figure is available in the online journal.)

gas compression at the shock-wave front. The probable cause of the shock waves is an active-nucleus jet that penetrates the surrounding interstellar medium. Such intrusions are observed in many Seyfert galaxies, for example, in Mrk 3 (Capetti et al. 1999). Unfortunately, for NGC 7743 we have no narrow-filter emission-line images with a sufficiently high spatial resolution to inspect this peculiar region in detail. But Regan & Mulchaey (1999) mentioned a "blue-color excess" at 1″(∼90 pc) to the southeast of the nucleus in the *HST* map of the galaxy—this may be the region of the suggested jet intrusion. In this case, we only see the jet directed toward us, while the counterjet is obscured by the galaxy's disk.

A radio image of the jet would provide decisive proof for this suggestion. But, as we noted in Section 2, all radio-continuum maps of NGC 7743 demonstrate only its compact core. Perhaps the spatial resolutions and sensitivities of these radio observations are insufficient to resolve a jet.

6. DISCUSSION

Previously known data (see Section 2) characterized NGC 7743 as an ordinary early-type spiral galaxy with weak nuclear activity. The traces of nuclear jet intrusion (the size of the jet must be less than 200 pc) in the interstellar medium that we found are not so surprising for a Seyfert galaxy. However, another astonishing fact is revealed: the bulk of ionized gas, up to 4–5 kpc from the center, rotates on the orbits strongly inclined (by $\delta i = 34°$ or 78°) toward the plane of the stellar disk.

The large-scale disk of NGC 7743 lacks prominent H II regions, and the gas excitation we determined from the emission-line spectrum is shock-like. We observed a similar situation in NGC 5631 (Sil'chenko et al. 2009), where the large-scale gaseous disk is slightly inclined toward the stellar one and has an opposite spin. We suggested two possible origins of the shock-like excitation: it can be due to either the collisions between the accreted gaseous clouds on the inclined orbits, with the original low-density gaseous disk coplanar to the stellar one, or the accreted gas clouds crossing the gravitational well of the stellar disk. However, in any case, the gaseous content of the main galactic disk must be several times smaller than the accreted gas mass. Otherwise, we would see two-component emission-line profiles over the entire disk extension, not only in the jet region.

Unfortunately, we did not find any simulations of shock waves induced in inclined gaseous disks in the literature, except the estimations by Wakamatsu (1993) for the case of polar rings. However, qualitatively, we consider the mechanisms proposed above quite probable and similar to spiral density wave generation in large-scale gaseous disks of spiral galaxies, and to the shock-induced dust lanes at the leading edges of bars. These scenarios can also explain the complex gas velocity behavior in the inner part of NGC 7743: the large-scale bar of the galaxy does not affect the gas at large distances from the center but can affect its rotation at $R < 20''$.

Among the galaxies known as "polar-ring galaxies," we note several cases of strongly inclined rings. In NGC 660 the outer gas-dust ring is inclined by $\delta i = 63°$ to the main galactic disk (Arnaboldi & Galletta 1993). An inclined gaseous disk, less pronounced than that in NGC 660 and more similar to the case of NGC 7743, was recently found in Arp 212 by Moiseev (2008). In Arp 212, a set of H II regions within the radii of 2–6 kpc concentrates in the plane, which is inclined by $\delta i = 30°$–$50°$ with respect to the inner disk of the galaxy; in the regions where two disks cross, prominent shock fronts are seen. Moiseev (2008) suggested gas accretion from the neighboring gas-rich satellite as the most probable mechanism of the inclined-disk formation in Arp 212. Such a scenario for the formation of polar and inclined gaseous rings was first proposed by Reshetnikov & Sotnikova (1997) and greatly developed during the past few years; see Bournaud & Combes (2003). We think that a similar scenario provoked the formation of the gaseous disk in NGC 7743. An alternate explanation may be minor merging or even a disruption of a gas-rich satellite by tidal forces from NGC 7743. But the latter scenario would produce other consequences, such as kinematically decoupled stellar subsystems or outer shells and arcs, which are not observed in NGC 7743. We hence conclude that, in any case, a possible contribution by the accreted stellar component in NGC 7743 would be small, and we must come back to gas-dominated accretion as the probable cause of the present state of NGC 7743.

In Section 2, we mentioned that near NGC 7743 there are at least two gas-rich satellites, so there is no problem in identifying a source of gas accretion. Moreover, 50′ (279 kpc) from NGC 7743 is another S0 galaxy, NGC 7742; the systemic velocity of NGC 7742 differs from that of NGC 7743 by only 50 km s^{-1}. Let us imagine that, earlier, NGC 7742 and NGC 7743 approached each other with a typical relative velocity of 200 km s^{-1}; then, the time spent after this passage is about 1.4 Gyr. This time is comparable to the age of the nuclear star formation burst in NGC 7743 that may have been induced by this interaction. However, we doubt that the inclined gaseous

disk was formed during the same event because this inclined-disk configuration is dynamically unstable and cannot persist its inclined rotation during several periods. It is probable that the inclined-orbit gas was accreted more recently.

7. CONCLUSIONS

Using the data of deep long-slit spectroscopy, obtained via the Russian 6-m telescope and the archive data of the integral-field spectrograph SAURON, we studied the stellar population properties and kinematics of the stellar and ionized-gas components in the early-type disk galaxy NGC 7743. We report the following results.

1. All ionized gas at radii of 1.5–5.4 kpc is confined to the disk and inclined strongly toward the main stellar disk of NGC 7743. The angle between two disks is estimated; two possible solutions are obtained, $34^\circ \pm 9^\circ$ or $77^\circ \pm 9^\circ$, depending on the mutual disk orientation in space. The most probable origin of this inclined gaseous disk is the accretion from the gas-rich environment of NGC 7743. The main contributor to gas excitation is the shock waves, probably induced by inclined-orbit gas clouds, that cross the main stellar disk.
2. Complex motions, multi-component emission-line profiles, and strong shock excitation of the gas inside a compact region 1″–2″ to the south of the nucleus are interpreted by us as the signatures of active-nucleus jet interaction with the surrounding ambient medium.
3. We confirm the recent (about 1 Gyr ago) intense star formation burst in the very center of NGC 7743, perhaps stimulated by the tidal interaction with the neighboring NGC 7742.

The inclined gaseous disk in NGC 7743 has one of the lowest contrasts among the structures of this kind discovered in external galaxies. We think that deep spectroscopy of other gas-poor, early-type disk galaxies would allow one to find many such inclined gaseous disks, which are formed by gas accretion from external sources.

This research is partly based on the data obtained from the Isaac Newton Group Archive, which is maintained as part of the CASU Astronomical Data Centre at the Institute of Astronomy, Cambridge. We made use of the NASA/IPAC Extragalactic Database (NED), which is operated by the Jet Propulsion Laboratory, California Institute of Technology, under contract with the National Aeronautics and Space Administration. We acknowledge the usage of the HyperLeda database. This work was supported by the Russian Foundation for Basic Research (project No. 09-02-00870). A.V.M. is also grateful to the "Dynasty" Fund. The authors thank the anonymous referee for constructive advice that helped us improve the paper.

REFERENCES

Afanasiev, V. L., & Moiseev, A. V. 2005, Astron. Lett., 31, 193
Afanasiev, V. L., Sil'chenko, O. K., & Zasov, A. V. 1989, A&A, 213, L9
Allen, M. G., Groves, B. A., Dopita, M. A., Sutherland, R. S., & Kewley, L. J. 2008, ApJS, 178, 20
Alonso-Herrero, A., Rieke, M. J., Rieke, G. H., & Shields, J. C. 2000, ApJ, 530, 688
Arnaboldi, M., & Galletta, G. 1993, A&A, 268, 411
Bacon, R., Copin, Y., Monnet, G., et al. 2001, MNRAS, 326, 23
Bournaud, F., & Combes, F. 2003, A&A, 401, 817
Capetti, A., Axon, D. J., Macchetto, F. D., Marconi, A., & Winge, C. 1999, ApJ, 516, 187
Cappellari, M., Emsellem, E., & Krajnovic, D. 2011, MNRAS, 413, 813
Coccato, L., Corsini, E. M., Pizzella, A., & Bertola, F. 2007, A&A, 465, 777
Corsini, E. M., Pizzella, A., Coccato, L., & Bertola, F. 2003, A&A, 408, 873
Duprie, K., & Schneider, S. E. 1996, AJ, 112, 937
Erwin, P. 2005, MNRAS, 364, 283
Erwin, P., Pohlen, M., & Beckman, J. E. 2008, AJ, 135, 20
Ho, L. C., Filippenko, A. V., & Sargent, W. L. W. 1997, ApJS, 112, 315
Ho, L. C., & Ulvestad, J. S. 2001, ApJS, 133, 77
Jensen, J. B., Tonry, J. L., Barris, B. J., et al. 2003, ApJ, 583, 712
Katkov, I. Yu., & Chilingarian, I. V. 2011, in ASP Conf. Ser. 442, Astronomical Data Analysis Software and Systems XX, ed. I. N. Evans et al. (San Francisco, CA: ASP), 143
Kewley, L. J., Dopita, M. A., Sutherland, R. S., et al. 2001, ApJ, 556, 121
Koleva, M., Prugniel, Ph., Bouchard, A., & Wu, Y. 2009, A&A, 501, 1269
Koleva, M., Prugniel, Ph., & De Rijcke, S. 2008a, Astron. Nachr., 329, 968
Koleva, M., Prugniel, Ph., Ocvirk, P., Le Borgne, D., & Soubiran, C. 2008b, MNRAS, 385, 1998
Laurikainen, E., Salo, H., Buta, R., & Knapen, J. H. 2007, MNRAS, 381, 401
Le Borgne, D., Rocca-Volmerange, B., Prugniel, P., et al. 2004, A&A, 425, 881
Maiolino, R., Ruiz, M., Rieke, G. H., & Papadopoulos, P. 1997, ApJ, 485, 552
Martínez-Delgado, D., Gabany, R. J., Crawford, K., et al. 2010, AJ, 140, 962
Martini, P., Regan, M. W., Mulchaey, J. S., & Pogge, R. W. 2003, ApJS, 146, 353
Moiseev, A. V. 2008, Astrophys. Bull., 63, 201
Moiseev, A. V., Valdés, J. R., & Chavushyan, V. H. 2004, A&A, 421, 433
Nagar, N. M., Wilson, A. S., Mulchaey, J. S., & Gallimore, J. F. 1999, ApJS, 120, 209
Regan, M. W., & Mulchaey, J. S. 1999, AJ, 117, 2676
Reshetnikov, V., & Sotnikova, N. 1997, A&A, 325, 933
Sarzi, M., Falcón-Barroso, J., Davies, R. L., et al. 2006, MNRAS, 366, 1151
Sil'chenko, O. K. 2006, ApJ, 641, 229
Sil'chenko, O. K., & Chilingarian, I. V. 2011, Astron. Lett., 37, 1
Sil'chenko, O. K., Moiseev, A. V., & Afanasiev, V. L. 2009, ApJ, 694, 1550
Smirnova, A., & Moiseev, A. 2010, MNRAS, 401, 307
Smirnova, A. A., Moiseev, A., & Afanasiev, V. L. 2010, MNRAS, 408, 400
Stasińska, G., Cid Fernandes, R., Mateus, A., Sodré, L., & Asari, N. V. 2006, MNRAS, 371, 972
Terashima, Y., Iyomoto, N., Ho, L. C., & Ptak, A. F. 2002, ApJS, 139, 1
Veilleux, S., & Osterbrock, D. E. 1987, ApJS, 63, 295
Wakamatsu, K. 1993, AJ, 105, 1745
Wozniak, H., Combes, F., Emsellem, E., & Friedli, D. 2003, A&A, 409, 469
Zasov, A. V., Moiseev, A. V., Khoperskov, A. V., & Sidorova, E. A. 2008, Astron. Rep., 52, 79